The effects of Temperature on Ozone in urban conditions – a modelling study

J. Coates[1] and T. Butler[1]

[1]Institute for Advanced Sustainability Studies, Potsdam, Germany

December 28, 2015

Abstract

1 Introduction

Surface-level ozone (O_3) is a secondary air pollutant formed from the photochemical degradation of volatile organic compounds (VOCs) in the presence of nitrogen oxides (NO_x). Due to the photochemical nature of ozone production, meteorological factors such as temperature strongly influence ozone production (Jacob and Winner, 2009).

Temperature influences ozone production through temperature-dependent emissions of VOC from biogenic sources (anthropogenic emissions are typically not temperature dependent) and the reaction rates of many of the chemical reactions involved in producing ozone are also temperature dependent. The recent review of Pusede et al. (2015) provides a detailed description of the temperature-dependent processes impacting ozone production. A recent study by Otero et al. (2016) indicates that temperature is a major meteorological driver for ozone in central europe.

Many studies over the US (Sillman and Samson, 1995; Dawson et al., 2007; Pusede et al., 2014) have observed the relationship between ozone and temperature, noting that increased temperatures tend to lead to higher ozone levels, often exceeding local air quality guidelines. Some of these studies (Sillman and Samson, 1995; Dawson et al., 2007) include modelling experiments using regional chemical tranport models which have indeed verified the observed increases in

ozone with temperature. The increase in the thermal decomposition rate of PAN (peroxy acetyl nitrate) with temperature is commonly cited for the increase of ozone with temperature.

Environmental chamber studies have looked at the relationship of ozone with temperature using a particular mixture of VOCs. The chamber experiments of Carter et al. (1979) and Hatakeyama et al. (1991), also showed inreases in ozone with temperature and have also linked this relationship to increased PAN decomposition at higher temperatures (T >303 K). Hatakeyama et al. (1991) looked primarily at the influence of HO_2NO_2 decomposition on ozone production and induced that at lower temperatures (T < 303 K) HO_2NO_2 decomposition has a large influence on ozone production but the influence of PAN decomposition on ozone production increases with temperature.

Pusede et al. (2014) used observations over the San Joaquin Valley, California to infer a non-linear relationship of ozone production with temperature and NO_x, similar to the well-known non-linear relationship of ozone production on NO_x and VOC levels (Sillman, 1999). In fact, Pusede et al. (2014) show that temperature can be used as a surrogate for VOC levels when looking at the relationship of ozone across NO_x gradients. Moreover, the described relationship of ozone on both NO_x and temperature needs to be considered when looking at effective stratgies to reduce levels of surface ozone.

Despite a wealth of studies looking at the effects of temperature on ozone chemistry, there have not been (to our knowledge) modelling studies focusing on these effects across different NO_x gradients and whether the observed relationships are well-represented by different chemical mechanisms used in air quality models. The review of Pusede et al. (2015) also highlights a lack of modelling studies looking at this non-linear relationship of ozone on temperature across NO_x gradients. In this study, we use an idealised box model to determine how ozone levels vary with temperature and across NO_x gradients. We separate the effects of temperature-dependent chemistry and VOC emissions on ozone production by performing simulations including a temperature-independent source of isoprene followed by simulations using a temperature-dependent source of isoprene.

The study of Rasmussen et al. (2013) looking at the change of ozone with temperature in California (termed the "Ozone-Climate Penalty") indicates that changing the chemical mechanism used by a model may also change the Ozone-Climate Penalty and should be investigated. Finally, by repeating these simulations with different chemical mechanisms, we determine whether the temperature dependence of ozone production is reproduced across different NO_x gradients in

these chemical mechanisms.

2 Methodology

2.1 Model Setup

All simulations were performed using the MECCA box model, originally described in Sander et al. (2005), as set up in Coates and Butler (2015) to broadly simulate urban conditions of central Europe. In this study, MECCA box model was further updated to include vertical mixing with the free troposphere and included a diurnal cycle for the PBL height based on the data from the BAERLIN 2014 campaign over Berlin, Germany (Bonn and et.al., 2016). The supplementary material includes further details about these updates.

Simulations were performed using equinoctical conditions and started at 06:00 with a run time of two days. Methane was fixed at 1.7 ppmv throughout the model run, carbon monoxide (CO) and ozone were initialised at 200 ppbv and 40 ppbv and then allowed to evolve freely throughout the the simulation. All VOC emissions were held constant until noon of first day, to simulate a plume of emitted VOC.

Model runs were repeated using a temperature-dependent and temperature-independent source of biogenic VOC (BVOC) emissions. MEGAN2.1 (Guenther et al., 2012) was used to specify the temperature-dependent BVOC emissions of isoprene, Sect. 2.3 provides further details. We focus only on isoprene as isoprene is the most important BVOC on the global scale due its high emission rates and emissions from vegetation are dependent on temperature (Guenther et al., 2006). In reality, increased temperature can also increase anthropogenic VOC (AVOC) emissions through increased evaporation.

All simulations were repeated using different chemical mechanisms to investigate how well the relationship of ozone with temprature across NO_x gradients is represented. The reference chemical mechanism is the near-explicit Master Chemical Mechanism, MCMv3.2, (Jenkin et al., 1997), (Jenkin et al., 2003), (Saunders et al., 2003), (Rickard et al., 2015). The reduced chemical mechanisms in our study are Common Representative Intermediates, CRIv2 (Jenkin et al., 2008), Model for ozone and related chemical tracers, MOZART-4 (Emmons et al., 2010), Regional Acid Deposition Model, RADM2 (Stockwell et al., 1990) and the Carbon Bond Mechanism, CB05 (Yarwood et al., 2005). Coates and Butler (2015) describes these chemical mechanisms and the implementation of these chemical mechanisms in MECCA. These reduced chemical mechanisms

Table 1: Total AVOC emissions in 2011 in tonnes from each SNAP category assigned from TNO-MACC_III emission inventory and temperature-independent biogenic VOC emission in tonnes from Benelux region assigned from EMEP. The allocation of these emissions to MCMv3.2, CRIv2, CB05, MOZART-4 and RADM2 species is found in the supplementary material.

	SNAP1	**SNAP2**	**SNAP34**	**SNAP5**	**SNAP6**	**SNAP71**
Belgium	4494	9034	22152	5448	42809	6592
Netherlands	9140	12173	29177	8723	53535	16589
Luxembourg	121	44	208	1371	4482	1740
Total	13755	21251	62648	15542	100826	24921
	SNAP72	**SNAP73**	**SNAP74**	**SNAP8**	**SNAP9**	**BVOC**
Belgium	2446	144	210	6448	821	7042
Netherlands	3230	1283	1793	10067	521	1462
Luxembourg	1051	6	324	643	0	2198
Total	6727	1433	2327	17158	1342	10702

were chosen as they are commonly used by modelling groups in 3D regional and global models.

The temperature was systematically varied between 288 and 313 K (15 – 40 °C). The only source of NOx emissions in the box model was a constant source of NO emissions. The NO emissions were systematically varied from 5.0 $\times$ 10^9 to 1.5 $\times$ 10^{12} molecules (NO) cm^{-2} s^{-1} at each temperature used in this study.

2.2 VOC Emissions

Typical emissions of urban AVOC over central Europe were taken from TNO-MACC_III emission inventory from the Benelux (Belgium, Netherlands and Luxembourg) region for the year 2011. TNO-MACC_III is the current version of the TNO-MACC_II inventory created using the same methodology as Kuenen et al. (2014) and based upon improvements to the existing emission inventory during the AQMEII-2 exercies described in Pouliot et al. (2015).

Temperature-independent emissions of the biogenic VOC isoprene and monoterpenes, were calculated as a fraction of the total AVOC emissions from each country in the Benelux region. This data was obtained from the supplementary data available from the EMEP (European Monitoring and Evaluation Programme) model (Simpson et al., 2012). Temperature-dependent emissions of isoprene are detailed in Sect. 2.3.

The AVOC emissions from the emission inventory were allocated to SNAP (Selected Nomenclature for Air Pollution) source categories and these category emissions were assigned to chemical species and groups based on the country specific profiles for Belgium, the Netherlands and Luxembourg provided by TNO. Table 1 shows the tonnes of NMVOC emissions from each

SNAP category and the temperature-independent BVOC emissions.

In order to represent the AVOC emissions from each SNAP category in the MCMv3.2, the same approach as described in von Schneidemesser et al. (2016) was used. In summary, most individual chemical species are represented by the MCMv3.2 otherwise the individual contributions of a group of NMVOC were further split into individual components using the detailed speciation of Passant (2002). For example, 'xylenes' are one of the component chemical groups to many SNAP categories but the MCMv3.2 treats xylenes by the individual isomers (m-, o-, p-xylene) and the individual contributions of the individual isomers to a SNAP category was provided by Passant (2002).

Again similarly to von Schneidemesser et al. (2016), the NMVOC emissions were first assigned to chemcial species represented by the MCMv3.2 and then mapped to the mechanism species representing NMVOC emissions in the reduced chemical mechanisms. The NMVOC emissions in the reduced chemical mechanisms were weighted by the carbon numbers of the MCMv3.2 species and the emitted mechanism species. The supplementary data outlines the primary NMVOC and calculated emissions with each chemical mechanism.

2.3 Temperature Dependent Isoprene Emissions

Temperature-dependent emissions of isoprene were estimated using the MEGAN2.1 model for calculating the emissions of VOC from vegetation (Guenther et al., 2012). Emissions from plants are dependent on variables including temperature, radiation and age but for the purpose of our study we are only interested in the effects of temperature, hence all variables except temprature were held constant.

The MEGAN2.1 parameters were chosen to give similar isoprene mixing ratios at 20 °C to the temperature-independent emissions, enabling an adequate comparison of the effects of increased isoprene emissions from the temperature-independent case. The estimated emissions of isoprene with MEGAN2.1 using these assumptions, are illustrated in Fig. 1 and show the expected exponential increase in emissions with temperature (Guenther et al., 2006).

To verify whether our inputs to calculating isoprene emissions using MEGAN2.1, we compare the simulated isoprene mixing ratios to those measured from over the urban area of Essen, Germany (Wagner and Kuttler, 2014). At 20 °C, the estimated emissions of isoprene lead to 0.07 ppbv of isoprene in our model while at 30 °C, the increased emissions of isoprene using MEGAN2.1 estimations lead to 0.35 ppbv of isoprene in the model. In the measurement campaign

Figure 1: The estimated isoprene emissions (molecules isoprene cm^{-2} s^{-1}) at each temperature step used in the study. Isoprene emissions were estimated using the MEGAN2.1 algorithm (Guenther et al., 2012).

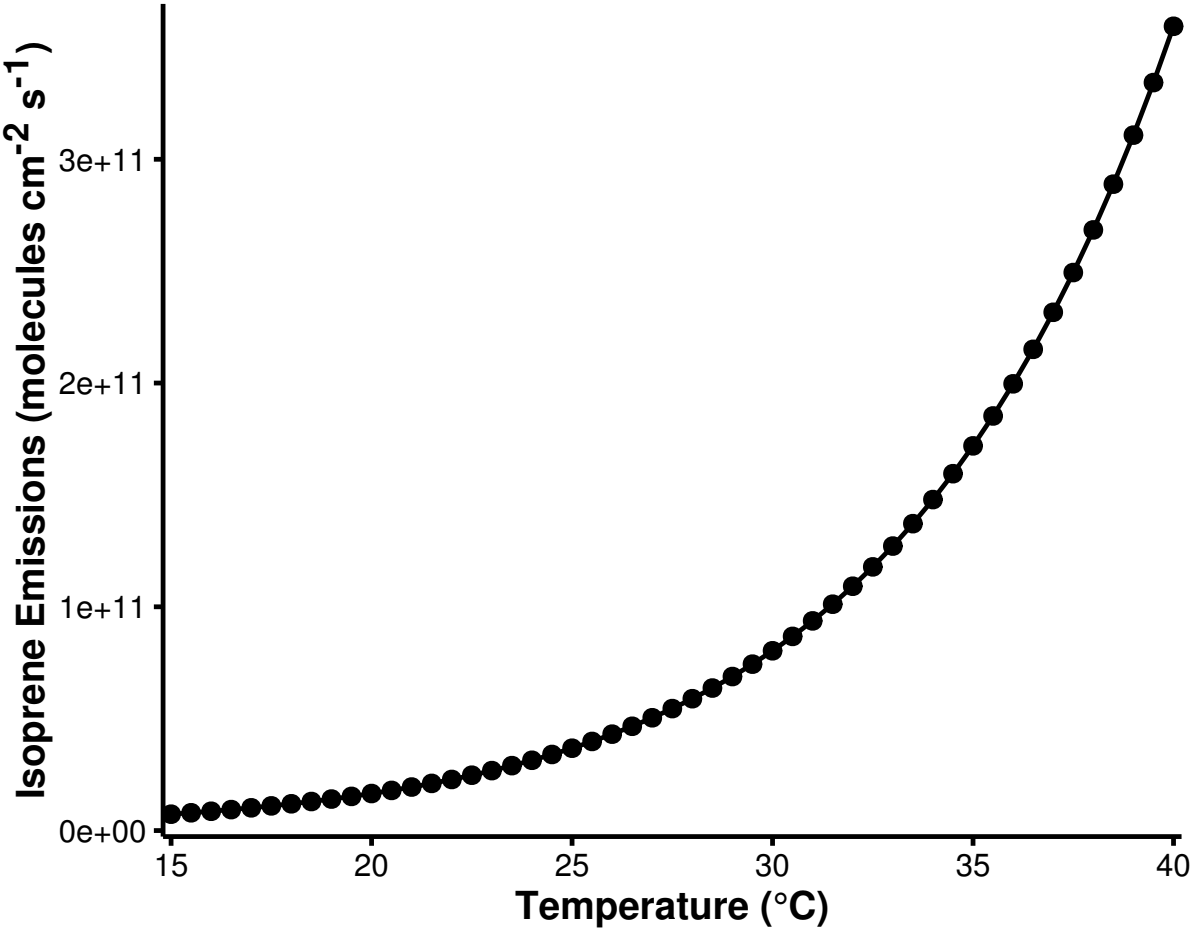

over Essen, 0.1 ppbv of isoprene were measured at temperatures of 20 °C and 0.3 ppbv of isoprene were measured at 30 °C. This comparison indicates that the values chosen for calculating the temperature-dependent emissions of isoprene with MEGAN2.1 lead to reasonable values of isoprene mixing ratios.

3 Results and Discussion

3.1 Ozone mixing ratios as function of NOx and Temperature

Figure 2 depicts the maximum mixing ratio of ozone as a function of the total NO_x emissions on the first day and temperature when using temperature-independent and temperature-dependent source of isoprene emissions for each chemical mechanism. A non-linear relationship of ozone mixing ratios with NO_x and temperature is reproduced by each chemical mechanism. This non-linear relationship has a similar form to that determined by Pusede et al. (2014) using an

Figure 2: Contours of maximum ozone mixing ratio as a function of the total NO_x emissions on the first day and temperature for each chemical mechanism and using both a temperature-dependent and -independent source of isoprene emissions.

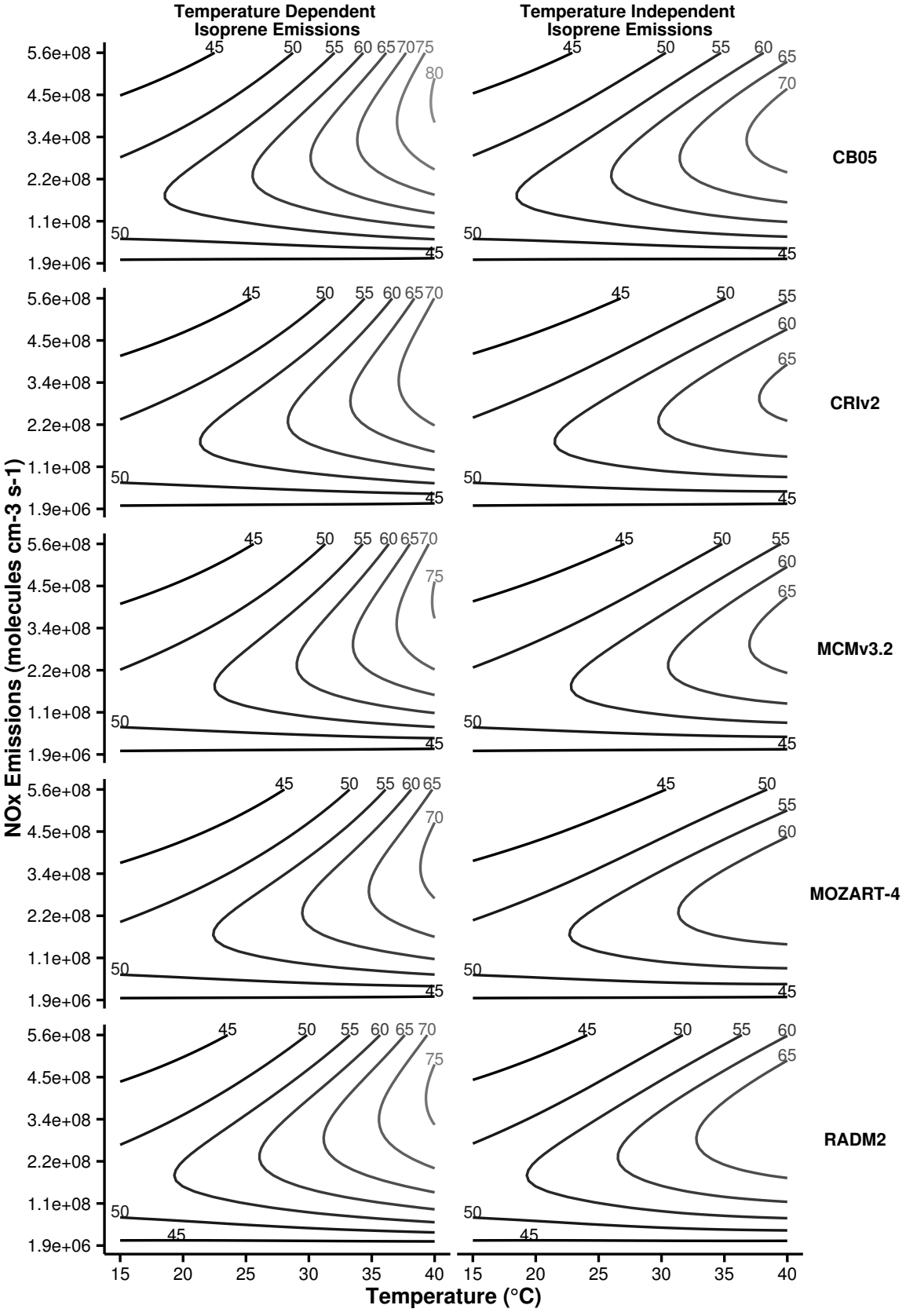

Figure 3: Ozone mixing ratios at each temperature are allocated to different NO_x-regimes of Fig. 2. The differences in ozone mixing ratios due to chemistry and emissions of Table 2 are represented graphically for MOZART-4, the approach was used to calculate the differences with each chemical mechanism.

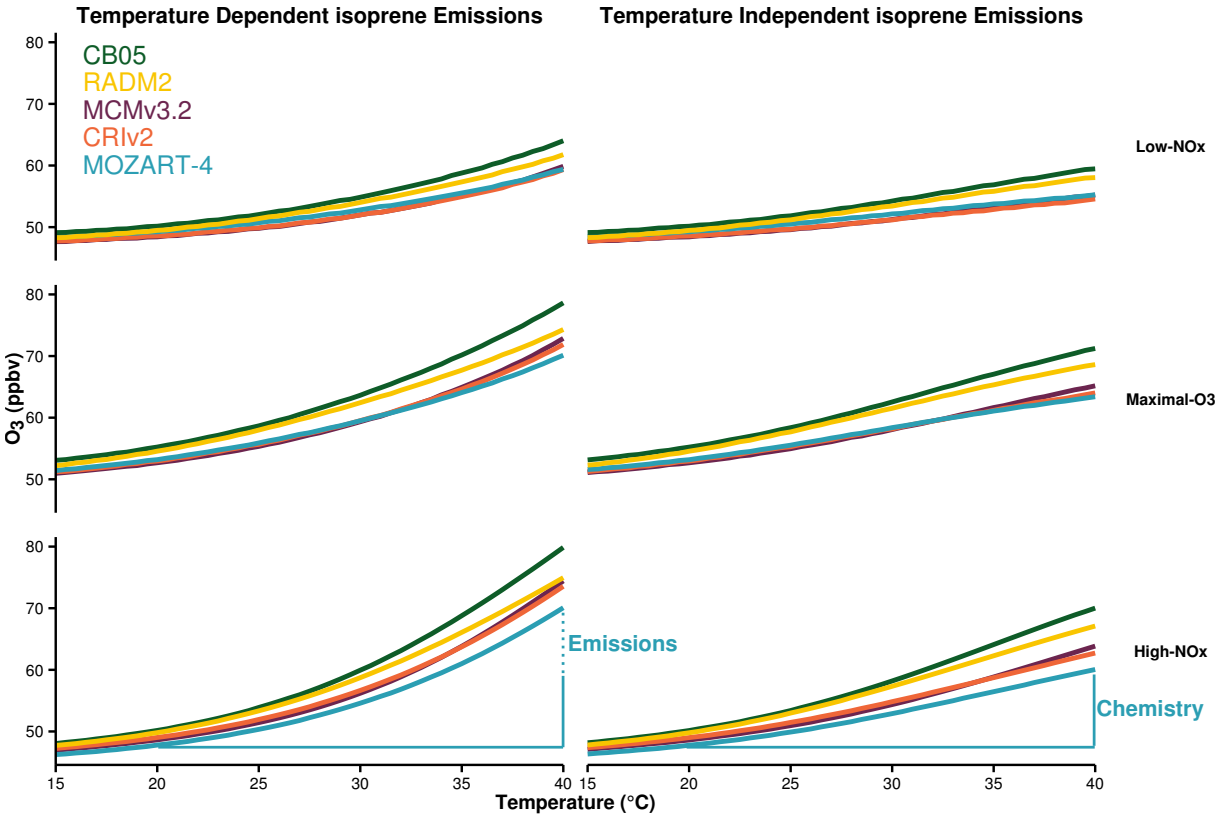

analytical model constrained to observational measurements over the San Joaquin Valley in California.

The highest mixing ratios of ozone in Fig. 2 are produced at higher temperatures and high-NO_x conditions, also ozone mixing ratios increase when using a temperature-dependent source of isoprene emissions. Conversely, the least amount of ozone is produced with low-NO_x conditions over the whole temperature range (15 – 40 °C) when using both a temperature-independent and temperature-dependent source of isoprene emissions.

The non-linear relationship of ozone with NO_x and temperature can be split into three NO_x-regimes (low-NO_x, maximal-O_3 and high-NO_x) based on the ratio of HNO_3 to H_2O_2 used in Sillman (1995) to determine NO_x-regimes for the non-linear relationship of ozone with NO_x and VOC. The low-NO_x regime corresponds to the lower-left most area in Fig. 2 where there is little increase in ozone with temperature, also called NO_x-sensitive conditions. The high-NO_x regime is when ozone levels increase rapidly with temperature in Fig. 2, sometimes called NO_x-saturated conditions. Finally, the ridges of the contours in Fig. 2 correspond to maximal-ozone production and we call this the maximal-O_3 regime. The ozone mixing ratios obtained in each simulation

Table 2: Increase in ozone mixing ratio (ppbv) due to chemistry and emissions at 40 °C from reference temperature (20 °C) in the NO_x-regimes of Fig. 2.

Chemical Mechanism	**Source of Difference**	**Increase in Ozone at 40 °C from 20 °C (ppbv)**		
		Low-NO_x	**Maximal-O_3**	**High-NO_x**
MCMv3.2	Chemistry	6.8	12.5	15.2
	Emissions	4.6	7.7	10.6
CRIv2	Chemistry	6.0	11.1	13.7
	Emissions	4.8	7.9	10.8
MOZART-4	Chemistry	6.0	10.2	12.3
	Emissions	4.1	6.7	10.0
CB05	Chemistry	9.3	16.0	19.9
	Emissions	4.6	7.4	9.8
RADM2	Chemistry	8.6	14.1	17.3
	Emissions	3.8	5.7	7.8

were assigned to a NO_x regime based on the H_2O_2:HNO_3 of the simulation and Fig. 3 illustrates the mean ozone mixing ratio at each temperature in these NO_x regimes.

Calculating the difference in ozone mixing ratios at 40 °C from 20 °C when using a temperature-independent source of isoprene emissions gives the absolute increase in ozone due to faster chemistry. When using a temperature-dependent source of isoprene emissions, the difference in ozone mixing ratios at 40 °C from 20 °C less the increase due to faster chemistry, gives the absolute increase in ozone due to increased isoprene emissions. These differences are represented graphically in Fig. 3 and summarised in Table 2.

Both Fig. 3 and Table 2 highlight that the absolute increase in ozone at 40 °C from 20 °C is largest with high-NO_x conditions. The increase in ozone mixing ratio at 40 °C from 20 °C due to faster chemistry with high-NO_x conditions is almost double that with low-NO_x conditions. We shall explore which chemical processes are responsible for the increases in ozone mixing ratios at 40 °C from 20 °C by analysing O_x production budgets in Sect. 3.2.

Comparing the response of ozone mixing ratios to temperature in the reduced chemical mechanisms (CRIv2, MOZART-4, CB05 and RADM2) to the near-explicit MCMv3.2 chemical mechanism shows that the largest differences from the MCMv3.2 occur in the maximal-O_3 and high-NO_x regimes. Table 2 also indicates that all reduced chemical mechanisms, except RADM2, have similar increases in ozone due to temperature-dependent isoprene emissions to MCMv3.2. RADM2 produces 3 ppbv less ozone than the MCMv3.2 due to temperature-dependent isoprene emissions consistently in each NO_x regime, indicating that this difference is due to how isoprene degradation chemistry is treated in RADM2.

The Tagged Ozone Production Potential (TOPP) of isoprene is a measure of the number

of molecules of ozone produced per molecule of isoprene emitted and Coates and Butler (2015) shows that less ozone is produced from isoprene degradation using RADM2 than with MCMv3.2. The degradation of isoprene has been extensively studied and it is well-known that the species methyl vinyl ketone (MVK) and methacrolein are signatures of isoprene degradation. All chemical mechanisms used in our study do explicitly include MVK and methacrolein (or in the case of CB05, a lumped species representing both these secondary degradation products) production during isoprene degradation except RADM2. RADM2 does not include methacrolein and the ketone species included in RADM2 represents a mixture of acetone and methyl ethyl ketone (MEK), thus the secondary degradation of isoprene in RADM2 is unable to represent the ozone production from the further degradation of its signature degradation products MVK and methacrolein. More recent versions of RADM2, RACM (Stockwell et al., 1997) and RACM2 (Goliff et al., 2013), sequentially include methacrolein and MVK and with these updates the TOPP values of isoprene reported in Coates and Butler (2015) are similar to the TOPP value of isoprene in the MCMv3.2.

3.2 Ozone Production Budgets

In order to determine which chemical processes are causing the increase in ozone with temperature (Sect. 3.1), we analyse the O_x production budgets in each NO_x regime (low-NO_x, Maximal-O_3 and high-NO_x) defined in Sect. 3.1. We defined the O_x family to consist of O_3, NO_2 and O, and Fig. 4 displays the total day-time O_x production budgets normalised by the total initial oxidation rates of the emitted NMVOC for each chemical mechanism within each NO_x regime. The O_x production budgets in Fig. 4 are allocated to the major sources, where 'HO2', 'RO2', 'ARO2' represent the reactions of NO with HO_2, alkyl peroxy radicals and acyl peroxy radicals respectively. 'RO2NO2' represents the thermal decomposition of peroxy nitrates, 'Inorganic' represents all inorganic contributions to the O_x production budgets (primarily the de-excitation of O^1D to O) and any other remaining organic reactions producing O_x are included in the 'Other Organic' category.

In Fig. 4 the number of molecules of O_x produced per molecule of NMVOC oxidised in High-NO_x conditions is similar when using temperature-dependent or temperature-independent isoprene emissions for each chemical mechanism; the same is also true for the Maximal-O_3 and Low-NO_x regimes. Thus the increases in isoprene emissions in the temperature-dependent simulations are balanced by the faster oxidation rates of the emitted NMVOC. The highest amount of O_x is produced in the High-NO_x regime and the lowest amount of O_x is produced in

Figure 4: Day-time O_x production budgets normalised by the total oxidation rate of emitted VOC in the NO_x-regimes of Fig. 2. The budgets are allocated to the categories of inorganic reactions, peroxy nitrate (RO2NO2) decomposition, reactions of NO with HO2, alkyl peroxy radicals (RO2) and acyl peroxy radicals (ARO2). All other reactions contributing to O_x budgets are allocated to 'Other Organic'.

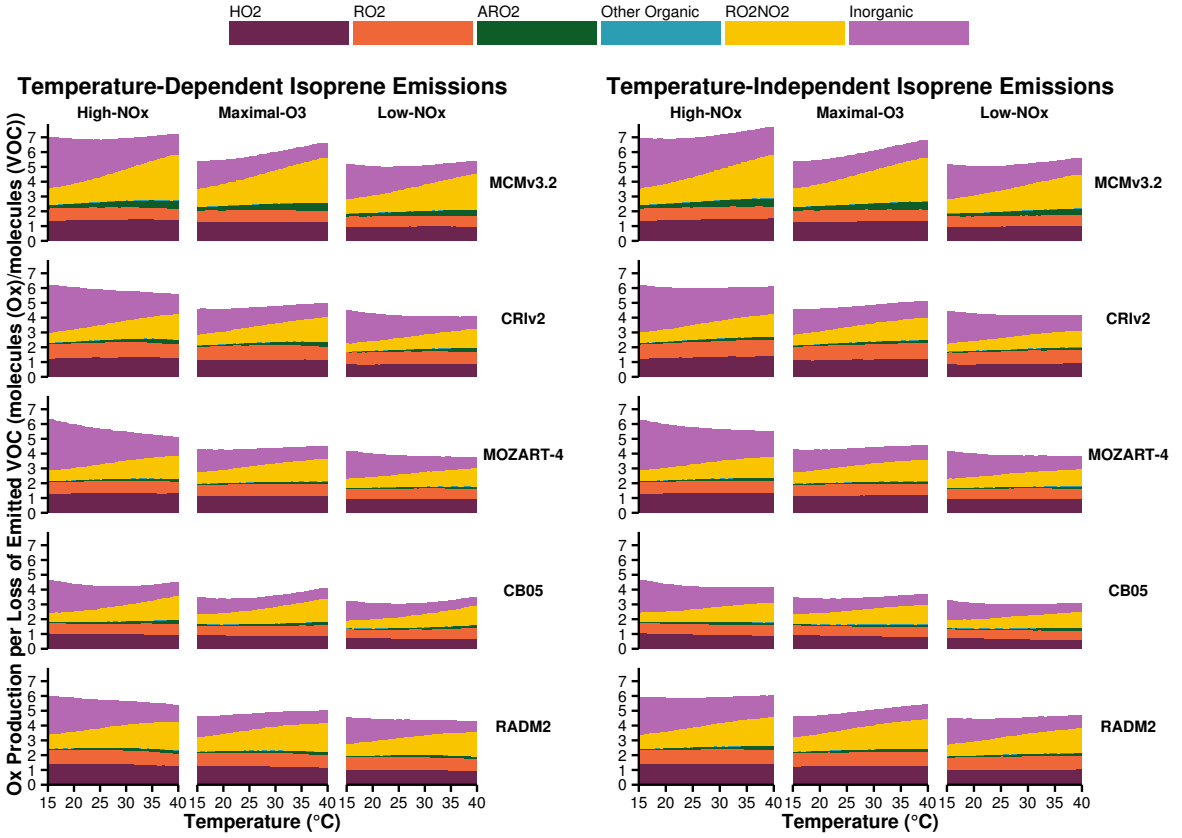

the Low-NO_x regime, mirroring the O_3 mixing ratios in the different NO_x regimes in Fig.3. For example, when using MCMv3.2 seven molecules of O_x are produced per molecule of NMVOC oxidation in High-NO_x conditions, decreased to about six and five molecules of O_x produced per molecule of NMVOC oxidised in the Maximal-O_3 and Low-NO_x regimes. In each NO_x regime, all the reduced chemical mechanisms produce up to two molecules of O_x per molecule of emitted NMVOC oxidised less than the MCMv3.2.

Turning to the individual contributions to the normalised production of O_x in Fig. 4, peroxy nitrate (RO2NO2) decomposition and inorganic reactions show a strong (and opposing) dependence on temperature in all NO_x regimes, each chemical mechanism and regardless of the source of isoprene emissions. Whereas the contributions of the reaction of NO with the peroxy radicals (HO2, RO2 and ARO2 in Fig. 4) to the normalised production budgets of O_x do not increase strongly with temperature indicating that these processes are strongly related to the faster oxidation of the emitted NMVOC with temperature.

3.2.1 Peroxynitrates

We shall now turn our focus to the peroxy nitrate (RO2NO2) contribution as this category has a strongly temperature-dependent contribution to the normalised O_x production. Peroxy nitrates are an important reservoir species for both peroxy radicals and NO_x that are formed from the reactions of alkyl and acyl peroxy nitrates with NO_2 (Reaction R1).

$$RO_2 + NO_2 + M \rightleftharpoons RO_2NO_2 + M \quad \text{(R1)}$$

The chemical bond of RO_2NO_2 is quite weak with thermal decomposition being the most important chemical reaction and thermal decomposition depends strongly on temperature. At low temperatures, RO_2NO_2 can accumulate and be transported downwind of emissions of the sources of its precursors (NMVOC and NO_x), after thermal decomposition the release of NO_2 and peroxy radicals can promote production of O_3 downwind (Moxim et al., 1996).

Peroxy nitrates are formed from both alkyl and acyl peroxy radicals, with the acyl peroxy radicals being more thermally stable than the alkyl peroxy nitrates. The most important alkyl peroxy nitrates are pernitric acid (HO_2NO_2) and methylperoxy nitrate ($CH_3O_2NO_2$), while peroxy acetyl nitrate (PAN, $CH_3C(O)O_2NO_2$) and peroxy propionyl nitrate (PPN, $C_2H_5C(O)O_2NO_2$) are important acyl peroxy nitrates.

The alkyl peroxy nitrates have a weaker $RO_2{-}NO_2$ bond than acyl peroxy nitrates hence alkyl peroxy nitrates have a shorter lifetime than acyl peroxy nitrates. For example, $CH_3O_2NO_2$ has a lifetime of 0.5 seconds at 298 K while PAN has a lifetime of 51 minutes at 298 K (Orlando and Tyndall, 2012).

Each chemical mechanism used in our study represents HO_2NO_2 and PAN, although in many reduced chemical mechanisms PAN represents $CH_3C(O)O_2NO_2$ and other acyl peroxy nitrates. This representation of PAN in reduced chemical mechanisms can lead to overestimations of PAN levels compared to more detailed chemical mechanisms (Luecken et al., 1999). The near-explicit MCMv3.2 represent a diverse range of peroxy nitrates including $CH_3O_2NO_2$ and about 280 acyl peroxy nitrates.

Figure 5 displays the normalised production budgets of RO_2NO_2 by the total loss rate of the emitted NMVOC, similar to Fig. 4 for each chemical mechanism in each NO_x regime and when using a temperature-independent and temperature-dependent source of isoprene emissions. The large contribution of $CH_3O_2NO_2$ in MCMv3.2 is not mirrored in any reduced chemical

Figure 5: Day-time RO_2NO_2 production budgets normalised by the total oxidation rate of emitted VOC in the NO_x-regimes of Fig. 2. The total budgets are allocated to the most important peroxy nitrates and all other contributions included as 'Others'.

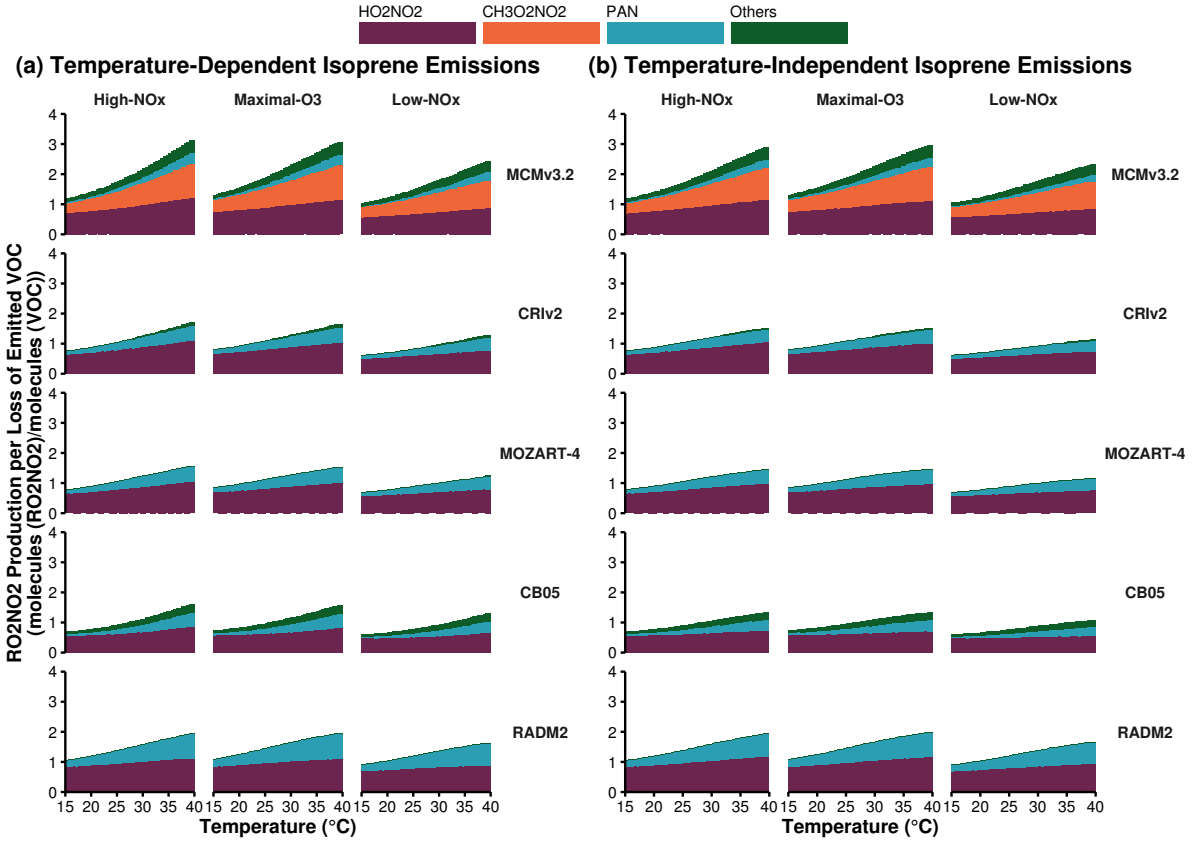

mechanism as $CH_3O_2NO_2$ is not represented in any of the reduced chemical mechanisms. In fact the number of molecules of RO_2NO_2 per molecules of NMVOC oxidised in each reduced chemical mechanism is very similar to that of MCMv3.2 less the contribution of $CH_3O_2NO_2$ for the separate NO_x regimes and regardless of isoprene source.

The contribution of RO2NO2 to the normalised O_x production in Fig. 4 is largest in the MCMv3.2 than the reduced chemical mechanisms due to the representation of $CH_3O_2NO_2$ in the MCMv3.2. If reduced chemical mechanisms represent $CH_3O_2NO_2$ chemistry then this would improve the representation of the total RO_2NO_2 production which would have the added effect of improving the representation of O_x production budgets.

3.3 Comparison to Observations and Regional Model Simulations

Our next aim was to compare the results from the detailed box model simulations of this study to real-world observations. The study of Otero et al. (2016) used the interpolated data set of Schnell et al. (2015) of the ERA-Interim re-analysis data set (Dee et al., 2011) which includes the daily maximum temperature and daily maximum 8-h mean of ozone for the years 1998–2012.

Figure 6: The maximum 8-h mean ozone from each box model experiment (temperature-dependent and temperature-independent isoprene emissions), allocated to the different NO_x regimes for each chemical mechanisms (solid lines). The box model ozone-temperature relationship is compared to the summer 2007 ERA-Interim data (black circles) and to WRF-Chem simulations using MOZART-4 (purple boxes) and RADM2 (orange triangles).

(a) Ozone-Temperature relationship over central and eastern Germany

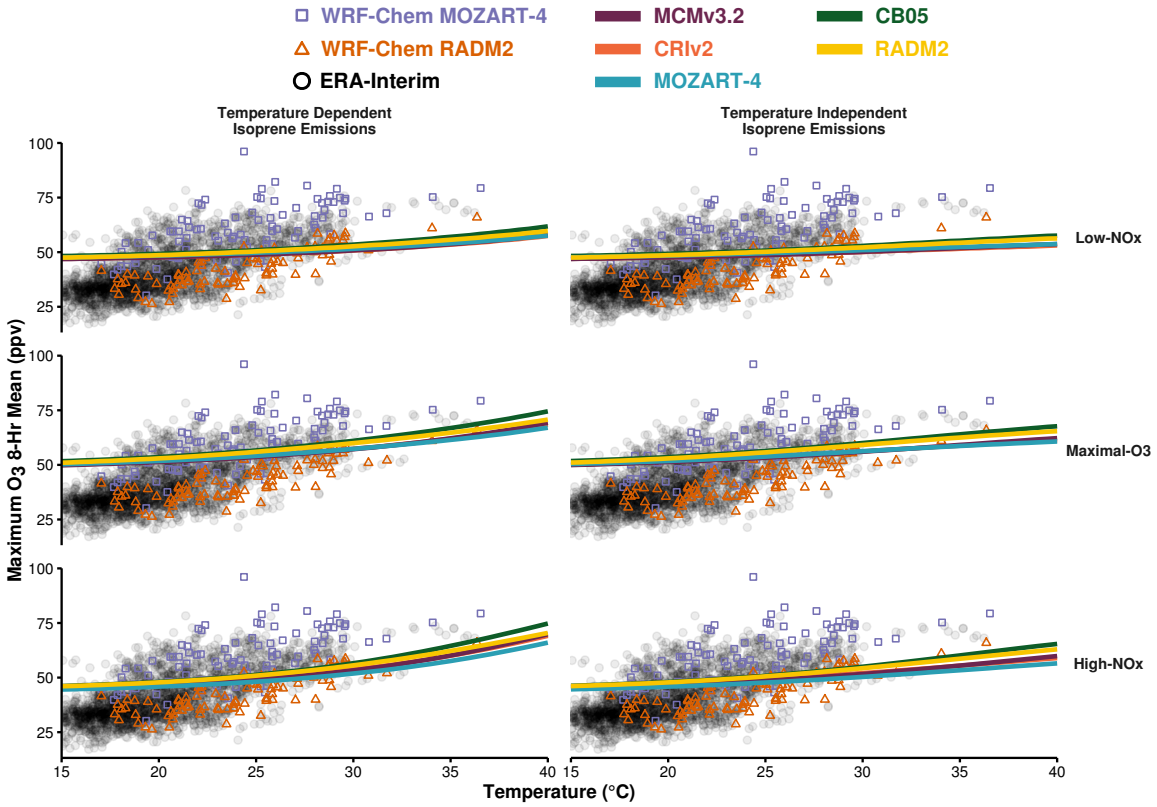

(b) Ozone-Temperature relationship over central and western Poland

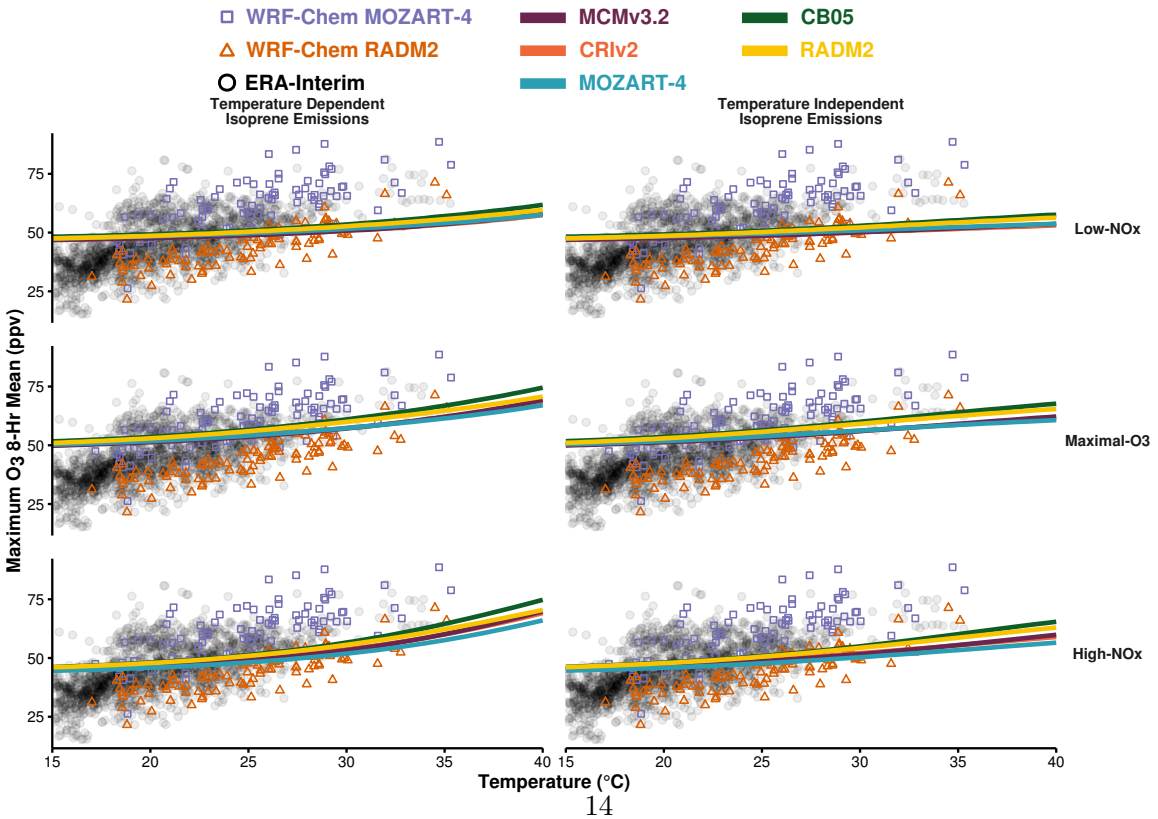

Table 3: Slopes ($m_{O3\text{-}T}$ in ppbv ozone per °C) of the linear fit to the ozone-temperature relationships displayed in Fig. 6

(a) Slope of linear fit of the ERA-Interim observational data and WRF-Chem model output using MOZART-4 and RADM2 chemistry over central and eastern Germany and western and central Poland.

	Germany	**Poland**
ERA-Interim	2.15	1.94
WRF-Chem with MOZART-4	2.05	2.00
WRF-Chem with RADM2	1.78	1.77

(b) Slope of linear fit of box model experiments for each chemical mechanism, type of isoprene emissions allocated to the three NO_x-regimes.

Mechanism	**Isoprene Emissions**	**Low-NO_x**	**Maximal-O_3**	**High-NO_x**
MCMv3.2	Temperature Dependent	0.42	0.74	0.93
	Temperature Independent	0.28	0.51	0.59
CRIv2	Temperature Dependent	0.40	0.71	0.90
	Temperature Independent	0.25	0.47	0.55
MOZART-4	Temperature Dependent	0.38	0.65	0.81
	Temperature Independent	0.25	0.44	0.49
CB05	Temperature Dependent	0.52	0.89	1.12
	Temperature Independent	0.39	0.67	0.79
RADM2	Temperature Dependent	0.48	0.79	0.97
	Temperature Independent	0.37	0.61	0.70

We were also in a position to compare our box model results to model simulations from the 3-D WRF-Chem regional model that was set-up over the European domain for the year 2007 using MOZART-4 and RADM2 chemistry . We have limited the ERA-Interim data to the summer (JJA) values as the Otero et al. (2016) study showed that summertime values of ozone over certain parts of central Europe are primarily driven by temperature and the year 2007 to provide a comparison with the WRF-Chem output.

Katie ref.

Figure 6 compares the summer 2007 data from observations (ERA-Interim), WRF-Chem model output and the maximum 8-hr mean ozone from the box model simulations using a temperature-independent and temperature-dependent source of isoprene emissions for each chemical mechanism and allocated to the different NO_x-regimes. We have selected two regions of the gridded domains for both the observations and WRF-Chem output to central and eastern Germany (Fig. 6a) and central and western Poland (Fig. 6b) as the summertime ozone values are correlated with temperature (Otero et al., 2016). Table 3 summarises the slopes ($m_{O3\text{-}T}$) of the linear fits of all the data displayed in Fig. 6 in ppbv of ozone per °C.

The large spread of the ERA-Interim ozone values over both Germany and Poland at the

different temperatures are well captured by the combined WRF-Chem simulations using both MOZART-4 and RADM2 chemistry. The ozone results from the WRF-Chem model using MOZART-4 chemistry re-produce the higher ozone values with temperature from ERA-Interim but not the lower values. On the other hand, the WRF-Chem simulations using RADM2 chemistry only reproduced the lower ozone values from the ERA-Interim data. The slopes of the WRF-Chem simulations using MOZART-4 chemistry are closer to the ERA-Interim data han the WRF-Chem simulations using RADM2 chemistry. However, the ozone values at the lower end of the temperature range (15–18 °C) are not simulated with the WRF-Chem model with either MOZART-4 or RADM2 chemistry.

The box model simulations using a temperature-independent source of isoprene emissions does not reproduce the spread of ozone-temperature data from ERA-Interim, also indicated by the $m_{O3\text{-}T}$ values in Table 3. When using a temperature-dependent source of isoprene emissions in the box model, the ozone-temperature values from the ERA-Interim data over Germany and Poland are reproduced slightly better as indicated by the $m_{O3\text{-}T}$ values in Table 3. The slopes from the box model results is best in the High-NO_x.

However, even in the box model results that have the most similar $m_{O3\text{-}T}$ to the ERA-Interim data, the slopes with the box model data are half that of the ERA-Interim data over both Germany and Poland. In particular, the box model ozone values at lower temperatures are over-predicted while the ozone values at higher temperatures are under-predicted to the ERA-Interim data.

One reason for the box model simulations being less sensitive to temperature than the observations are related to the set-up of the experiments. In our model set-up, we considered instantaneous ozone production from a freshly emitted emission plume at different temperatures whereas observational values would include ozone and temperature data resulting from other meteorological factors, in particular stagnant conditions. In stagnant conditions, the ozone built-up from the previous day is not transported away from the region and can lead to increased ozone levels with the production of fresh ozone from new emissions.

Observational studies look at the total effect of ozone with temperature, whereas a model can look at the temperature-dependent processes that influence ozone. In other words, observational studies look at the total derivative of ozone with temperature while models can look at the partial derivatives of the temperature-dependent processes influencing ozone.

$$\frac{d[O3]}{dT} = \frac{\partial[O3]}{\partial[BVOC]}\frac{\partial[BVOC]}{\partial T} + \frac{\partial[O3]}{\partial \mathrm{Chemistry}}\frac{\partial \mathrm{Chemistry}}{\partial T} + \frac{\partial[O3]}{\partial \mathrm{Stagnation}}\frac{\partial \mathrm{Stagnation}}{\partial T} + \dots$$

In our experiments, we have focused on determining whether chemistry or increased BVOC emissions are more important for the increase of ozone with temperature but further work including stagnation is also required. 3-D models such as WRF-Chem would play a valuable role for such further work as these models represent meteorology which is missing from our box model. Despite these short-comings of our box model set-up, the detailed analysis of the chemistry provided in this study should complement any future analysis of the ozone-temperature relationship.

4 Conclusions

References

B. Bonn and et.al. Mobile BAERLIN2014: Sources and sinks - The influence of land surface types and horizontal heterogeneity on air pollutant levels in Berlin. *In Preparation*, 2016.

William P. L. Carter, Arthur M. Winer, Karen R. Darnall, and James N. Pitts Jr. Smog chamber studies of temperature effects in photochemical smog. *Environmental Science & Technology*, 13 (9):1094–1100, 1979.

J. Coates and T. M. Butler. A comparison of chemical mechanisms using tagged ozone production potential (TOPP) analysis. *Atmospheric Chemistry and Physics*, 15(15):8795–8808, 2015.

John P. Dawson, Peter J. Adams, and Spyros N. Pandis. Sensitivity of ozone to summertime climate in the eastern USA: A modeling case study . *Atmospheric Environment*, 41(7):1494 – 1511, 2007.

D. P. Dee, S. M. Uppala, A. J. Simmons, P. Berrisford, P. Poli, S. Kobayashi, U. Andrae, M. A. Balmaseda, G. Balsamo, P. Bauer, P. Bechtold, A. C. M. Beljaars, L. van de Berg, J. Bidlot, N. Bormann, C. Delsol, R. Dragani, M. Fuentes, A. J. Geer, L. Haimberger, S. B. Healy, H. Hersbach, E. V. Hólm, L. Isaksen, P. Kållberg, M. Köhler, M. Matricardi, A. P. McNally, B. M. Monge-Sanz, J.-J. Morcrette, B.-K. Park, C. Peubey, P. de Rosnay, C. Tavolato, J.-N. Thépaut, and F. Vitart. The era-interim reanalysis: configuration and performance of the data assimilation system. *Quarterly Journal of the Royal Meteorological Society*, 137(656):553–597, 2011.

L. K. Emmons, S. Walters, P. G. Hess, J.-F. Lamarque, G. G. Pfister, D. Fillmore, C. Granier,

A. Guenther, D. Kinnison, T. Laepple, J. Orlando, X. Tie, G. Tyndall, C. Wiedinmyer, S. L. Baughcum, and S. Kloster. Description and evaluation of the Model for Ozone and Related chemical Tracers, version 4 (MOZART-4). *Geoscientific Model Development*, 3(1):43–67, 2010.

Wendy S. Goliff, William R. Stockwell, and Charlene V. Lawson. The regional atmospheric chemistry mechanism, version 2. *Atmospheric Environment*, 68:174 – 185, 2013.

A. Guenther, T. Karl, P. Harley, C. Wiedinmyer, P. I. Palmer, and C. Geron. Estimates of global terrestrial isoprene emissions using MEGAN (Model of Emissions of Gases and Aerosols from Nature). *Atmospheric Chemistry and Physics*, 6(11):3181–3210, 2006.

A. B. Guenther, X. Jiang, C. L. Heald, T. Sakulyanontvittaya, T. Duhl, L. K. Emmons, and X. Wang. The Model of Emissions of Gases and Aerosols from Nature version 2.1 (MEGAN2.1): an extended and updated framework for modeling biogenic emissions. *Geoscientific Model Development*, 5(6):1471–1492, 2012.

Shiro Hatakeyama, Hajime Akimoto, and Nobuaki Washida. Effect of temperature on the formation of photochemical ozone in a propene-nitrogen oxide (NOx)-air-irradiation system. *Environmental Science & Technology*, 25(11):1884–1890, 1991.

Daniel J. Jacob and Darrell A. Winner. Effect of climate change on air quality. *Atmospheric Environment*, 43(1):51 – 63, 2009. Atmospheric Environment - Fifty Years of Endeavour.

M. E. Jenkin, S. M. Saunders, V. Wagner, and M. J. Pilling. Protocol for the development of the Master Chemical Mechanism, MCM v3 (Part B): tropospheric degradation of aromatic volatile organic compounds. *Atmospheric Chemistry and Physics*, 3(1):181–193, 2003.

M.E. Jenkin, L.A. Watson, S.R. Utembe, and D.E. Shallcross. A Common Representative Intermediates (CRI) mechanism for VOC degradation. Part 1: Gas phase mechanism development. *Atmospheric Environment*, 42(31):7185 – 7195, 2008.

Michael E. Jenkin, Sandra M. Saunders, and Michael J. Pilling. The tropospheric degradation of volatile organic compounds: a protocol for mechanism development. *Atmospheric Environment*, 31(1):81 – 104, 1997.

J. J. P. Kuenen, A. J. H. Visschedijk, M. Jozwicka, and H. A. C. Denier van der Gon. TNO-MACC_II emission inventory; a multi-year (2003–2009) consistent high-resolution european

emission inventory for air quality modelling. *Atmospheric Chemistry and Physics*, 14(20): 10963–10976, 2014.

D.J. Luecken, G.S. Tonnesen, J.E. Sickles, and II. Differences in noy speciation predicted by three photochemical mechanisms. *Atmospheric Environment*, 33(7):1073 – 1084, 1999.

W. J. Moxim, H. Levy, and P. S. Kasibhatla. Simulated global tropospheric PAN: Its transport and impact on NO_x. *Journal of Geophysical Research: Atmospheres*, 101(D7):12621–12638, 1996.

John J. Orlando and Geoffrey S. Tyndall. Laboratory studies of organic peroxy radical chemistry: an overview with emphasis on recent issues of atmospheric significance. *Chem. Soc. Rev.*, 41: 6294–6317, 2012.

N. Otero, J. Sillmann, J. L. Schnell, H. Rust, and T. M. Butler. Synoptic and meteorological drivers of extreme ozone concentrations over europe. *Environmental Research Letters*, page In Preparation, 2016.

N. Passant. Speciation of UK emissions of non-methane volatile organic compounds. Technical report, DEFRA, Oxon, UK., 2002.

George Pouliot, Hugo A.C. Denier van der Gon, Jeroen Kuenen, Junhua Zhang, Michael D. Moran, and Paul A. Makar. Analysis of the emission inventories and model-ready emission datasets of Europe and North America for phase 2 of the AQMEII project. *Atmospheric Environment*, 115: 345–360, 2015.

S. E. Pusede, D. R. Gentner, P. J. Wooldridge, E. C. Browne, A. W. Rollins, K.-E. Min, A. R. Russell, J. Thomas, L. Zhang, W. H. Brune, S. B. Henry, J. P. DiGangi, F. N. Keutsch, S. A. Harrold, J. A. Thornton, M. R. Beaver, J. M. St. Clair, P. O. Wennberg, J. Sanders, X. Ren, T. C. VandenBoer, M. Z. Markovic, A. Guha, R. Weber, A. H. Goldstein, and R. C. Cohen. On the temperature dependence of organic reactivity, nitrogen oxides, ozone production, and the impact of emission controls in San Joaquin Valley, California. *Atmospheric Chemistry and Physics*, 14(7):3373–3395, 2014.

Sally E. Pusede, Allison L. Steiner, and Ronald C. Cohen. Temperature and Recent Trends in the Chemistry of Continental Surface Ozone. *Chemical Reviews*, 115(10):3898–3918, 2015.

D. J. Rasmussen, Jianlin Hu, Abdullah Mahmud, and Michael J. Kleeman. The ozone–climate

penalty: Past, present, and future. *Environmental Science & Technology*, 47(24):14258–14266, 2013. PMID: 24187951.

Andrew Rickard, Jenny Young, M. J. Pilling, M. E. Jenkin, Stephen Pascoe, and S. M. Saunders. The Master Chemical Mechanism Version MCM v3.2. `http://mcm.leeds.ac.uk/MCMv3.2/`, 2015. [Online; accessed 25-March-2015].

R. Sander, A. Kerkweg, P. Jöckel, and J. Lelieveld. Technical note: The new comprehensive atmospheric chemistry module mecca. *Atmospheric Chemistry and Physics*, 5(2):445–450, 2005.

S. M. Saunders, M. E. Jenkin, R. G. Derwent, and M. J. Pilling. Protocol for the development of the Master Chemical Mechanism, MCM v3 (Part A): tropospheric degradation of non-aromatic volatile organic compounds. *Atmospheric Chemistry and Physics*, 3(1):161–180, 2003.

J. L. Schnell, M. J. Prather, B. Josse, V. Naik, L. W. Horowitz, P. Cameron-Smith, D. Bergmann, G. Zeng, D. A. Plummer, K. Sudo, T. Nagashima, D. T. Shindell, G. Faluvegi, and S. A. Strode. Use of north american and european air quality networks to evaluate global chemistryâ€“climate modeling of surface ozone. *Atmospheric Chemistry and Physics*, 15(18):10581–10596, 2015.

Sanford Sillman. The use of NOy, H2O2, and HNO3 as indicators for ozone-NOx-hydrocarbon sensitivity in urban locations. *Journal of Geophysical Research: Atmospheres*, 100(D7): 14175–14188, 1995.

Sanford Sillman. The relation between ozone, NOx and hydrocarbons in urban and polluted rural environments. *Atmospheric Environment*, 33(12):1821 – 1845, 1999.

Sanford Sillman and Perry J. Samson. Impact of temperature on oxidant photochemistry in urban, polluted rural and remote environments. *Journal of Geophysical Research: Atmospheres*, 100(D6):11497–11508, 1995.

D. Simpson, A. Benedictow, H. Berge, R. Bergström, L. D. Emberson, H. Fagerli, C. R. Flechard, G. D. Hayman, M. Gauss, J. E. Jonson, M. E. Jenkin, A. Nyíri, C. Richter, V. S. Semeena, S. Tsyro, J.-P. Tuovinen, Á. Valdebenito, and P. Wind. The EMEP MSC-W chemical transport model – technical description. *Atmospheric Chemistry and Physics*, 12(16):7825–7865, 2012.

William R. Stockwell, Paulette Middleton, Julius S. Chang, and Xiaoyan Tang. The second generation regional acid deposition model chemical mechanism for regional air quality modeling. *Journal of Geophysical Research: Atmospheres*, 95(D10):16343–16367, 1990.

William R. Stockwell, Frank Kirchner, Michael Kuhn, and Stephan Seefeld. A new mechanism for regional atmospheric chemistry modeling. *Journal of Geophysical Research: Atmospheres*, 102(D22):25847–25879, 1997.

E. von Schneidemesser, J. Coates, A. J. H. Visschedijk, H. A. C. Denier van der Gon, and T. M. Butler. Variation of the NMVOC speciation in the solvent sector and the sensitivity of modelled tropospheric ozone. *Atmospheric Environment*, page In preparation, 2016.

Patrick Wagner and Wilhelm Kuttler. Biogenic and anthropogenic isoprene in the near-surface urban atmosphere — a case study in essen, germany. *Science of The Total Environment*, 475:104 – 115, 2014.

Greg Yarwood, Sunja Rao, Mark Yocke, and Gary Z. Whitten. Updates to the Carbon Bond Chemical Mechanism: CB05. Technical report, U. S Environmental Protection Agency, 2005.